

The Relationship between Atmospheric Convective Radiative Effect and Net Energy Transport in the Tropical Warm Pool

BRYCE E. HARROP AND DENNIS L. HARTMANN

Department of Atmospheric Sciences, University of Washington, Seattle, Washington

(Manuscript received 23 February 2015, in final form 11 August 2015)

ABSTRACT

Reanalysis data and radiation budget data are used to calculate the role of the atmospheric cloud radiative effect in determining the magnitude of horizontal export of energy by the tropical atmosphere. Because tropical high clouds result in net radiative heating of the atmosphere, they increase the requirement for the atmosphere to export energy from convective regions. Increases in upper-tropospheric water vapor associated with convection contribute about a fifth of the atmospheric radiative heating anomaly associated with convection. Over the warmest tropical oceans, the radiative effect of convective clouds and associated water vapor is roughly two-thirds the value of the atmospheric energy transport. Cloud radiative heating and atmospheric heat transport increase at the same rate with increasing sea surface temperature, suggesting that the increased energy export is supplied by the radiative heating associated with convective clouds. The net cloud radiative effect at the top of the atmosphere is insensitive to changes in SST over the warm pool. Principal component analysis of satellite-retrieved cloud data reveals that the insensitivity of the net cloud radiative effect to SST is the result of changes in cloud amount offsetting changes in cloud optical thickness and cloud-top height. While increasing upward motion makes the cloud radiative effect more negative, that decrease is offset by reductions in outgoing longwave radiation owing to increases in water vapor.

1. Introduction and background

The warm pool (10°S–10°N, 150°E–180°) is an area of active convection. Climatologically, it has the highest sea surface temperatures and strongest incoming top-of-the-atmosphere (TOA) net radiation. Additionally, the strongest atmospheric heat transport (AHT) out of the tropics occurs in the warm pool (Trenberth and Solomon 1994). The large-scale circulation ultimately controls the horizontal heat transport by the atmosphere, and convective heating plays an important role in determining the large-scale circulation. Convection is directly responsible for the vertical transport of moist static energy, and is also responsible for the generation of high clouds, whose radiative heating is another important contribution to the large-scale circulation.

Early studies using coarse grid general circulation model studies have shown the effects of cloud radiative heating within the atmosphere on the tropical circulation (see

Ramanathan 1987; Slingo and Slingo 1988, 1991; Randall et al. 1989; Sherwood et al. 1994). These studies showed that cloud radiative heating warms the upper tropical troposphere, accelerates the jet stream, enhances the mass flux in the mean meridional circulation, strengthens the Hadley and Walker circulations, increases precipitation, and can also excite extratropical height anomalies. Theoretical studies such as Stuhlmann and Smith (1988a,b) also suggested cloud radiative heating in the atmosphere will enhance the circulation patterns. Calculations of cloud radiative heating using International Satellite Cloud Climatology Project (ISCCP) data and European Centre for Medium-Range Weather Forecasts (ECMWF) analyses have found that cloud heating and cooling patterns reinforce the tropical circulations (Sohn 1999; Bergman and Hendon 2000b). Zhang and Rossow (1997) and Tian et al. (2001) noted that the heating of the clouds would, with all other things being equal, partition more of the net divergence of energy transport into the atmosphere instead of the ocean.

Clouds perturb the net radiative fluxes at the top of the atmosphere, termed the cloud radiative effect (CRE; see Table 1 for list of acronyms), as well as the surface (SCRE) and within the atmosphere (ACRE). In the

Corresponding author address: Bryce E. Harrop, Dept. of Atmospheric Sciences, University of Washington, Box 351640, Seattle, WA 98195-1640.
E-mail: bryce@atmos.washington.edu

TABLE 1. List of acronyms.

Acronym	Expansion
ACoRE	Atmospheric convective radiative effect
ACRE	Atmospheric cloud radiative effect
AHT	Atmospheric heat transport
AMRE	Atmospheric moisture radiative effect
CRE	Cloud radiative effect (at TOA)
EOF	Empirical orthogonal function
ERA-Interim	ECMWF interim reanalysis
LE	Surface latent heat flux
LWCRE	Longwave cloud radiative effect
MODIS	Moderate Resolution Imaging Spectroradiometer
OLR	Outgoing longwave radiation
PC	Principal component
SCRE	Surface cloud radiative effect
SFC	Surface
SH	Surface sensible heat flux
SST	Sea surface temperature
SWCRE	Shortwave cloud radiative effect

convective regions of the tropics the top-of-the-atmosphere net CRE is near zero (Ramanathan et al. 1989; Harrison et al. 1990; Kiehl and Ramanathan 1990; Kiehl 1994; Cess et al. 2001; Tian and Ramanathan 2002; Yuan and Hartmann 2008). The atmospheric and surface cloud radiative effects can be quite large in cloudy regions, however, owing primarily to the different ways shortwave and longwave radiation interact with clouds (Ramanathan 1987; Slingo and Slingo 1988; Ramanathan et al. 1989; Tian et al. 2001; Tian and Ramanathan 2002). ACRE is a large heating term for the atmosphere, especially in regions of persistent high clouds, while SCRE is a large cooling term for the surface (Ramanathan 1987; Slingo and Slingo 1988; Ramanathan et al. 1989; Harshvardhan et al. 1990; Sherwood et al. 1994; Tian et al. 2001; Tian and Ramanathan 2002). In the convective part of the tropics, ACRE and SCRE are largely offsetting, hence, the near-zero top-of-the-atmosphere CRE (Tian et al. 2001). Tian et al. (2001) suggest that the offsetting nature of the ACRE and SCRE allows them to be considered as an indirect energy transport; energy is lost at the surface and gained in the atmosphere. This indirect heat transport, as Tian et al. (2001) refer to it, adds to the direct transport from surface turbulent fluxes and moist convection. Sherwood et al. (1994) found that removing high cloud radiative heating reduced the Hadley circulation by about 25% (as measured by 500-hPa vertical velocity) while the Walker circulation completely collapsed. Bergman and Hendon (2000a) suggested that the cloud radiative heating in the atmosphere contributes about 20% to the overall circulation, as measured by the zonal mass flux.

The idea that ACRE drives AHT was further tested by Tian and Ramanathan (2002) and then again by Tian and Ramanathan (2003). Tian and Ramanathan (2002) showed that the mean spatial patterns of ACRE and AHT align well across the tropical Pacific, in terms of both structure and magnitude. Tian and Ramanathan (2003) showed that a model forced only by observed ACRE was capable of developing quantitatively realistic looking Hadley and Walker circulations. In contrast, forcing the model with surface evaporation created a wildly different circulation pattern compared to the real tropical atmosphere. Sohn (1999) suggested that water vapor convergence may act as a diabatic heating source like the clouds. Additionally, it was shown by Voigt et al. (2014) that shifts in the intertropical convergence zone (ITCZ) in aquaplanet simulations can be attributed to changes in the local cloud radiative heating within the atmosphere.

In this paper, we use the ERA-Interim output coupled with Clouds and the Earth's Radiant Energy System Energy Balanced and Filled (CERES-EBAF) data to estimate the ACRE, CRE, and horizontal energy divergence out of the tropical warm pool. Additionally, we explore the contributions to the radiative heating from convectively lofted water vapor, since its interactions with longwave radiation are similar to those of the clouds. We refer to this radiative heating anomaly as the atmospheric moisture radiative effect (AMRE). The combined ACRE and AMRE give us the atmospheric convective radiative effect (ACoRE), which is the total change in radiative cooling of the atmosphere due to the modification of the atmosphere's radiative properties by convection. We explore the relationship between ACoRE and energy divergence or AHT. While our results cannot show a causal relationship between ACoRE and AHT, we find that the two are closely related within the warm pool region. Our results confirm and elaborate on those of Tian et al. (2001) and Tian and Ramanathan (2002). We show that water vapor increases in convective regions make a substantial contribution to AHT. Our results are also consistent with Zelinka and Hartmann (2012), who showed that feedbacks within the climate system act to enhance the existing gradient in top-of-the-atmosphere radiative fluxes, and, hence, require stronger poleward heat transport. A more recent study by Lee and Yoo (2014) similarly suggests poleward heat transport being enhanced by the clouds. Our results are also consistent with work by Wu et al. (2011) and Hwang and Frierson (2010), in which increases in poleward energy transport in general circulation models are found to directly relate to changes in the gradient of moist static energy (MSE) within these models. Since the ACRE (and ACoRE) is a means of enhancing the

local MSE, it is likewise capable of enhancing poleward energy transport.

We further break down the ACoRE and AHT relationships across different thermodynamic and dynamic regimes. It is common to use sea surface temperature and pressure velocity along the 500-hPa surface as proxies (e.g., Bony et al. 1997, 2004; Yuan et al. 2008; Franklin et al. 2013). Additionally, we compare the rest of the tropics and several other regions (the western Pacific, eastern Pacific, Indian Ocean, and Atlantic Ocean) to the results found in the warm pool. We show that the structural relationships between ACoRE and AHT within the warm pool are common in all convective regions within the deep tropics (10°S–10°N). Additionally, we make use of MODIS data (Platnick et al. 2003) to investigate what types of cloud changes are occurring with respect to changes in sea surface temperature or vertical velocity. Principal component analysis of the MODIS data reveal that offsetting changes in cloud amount and cloud optical thickness make the cloud radiative effect insensitive to sea surface temperature in the tropical warm pool. Increases in upward vertical velocity, however, show increases in both cloud amount and cloud optical thickness, which decrease CRE.

2. Methods and datasets

We make use of the ERA-Interim (Dee et al. 2011) dataset to get the divergence terms as well as the SSTs. The reanalysis is run on a $0.75^\circ \times 0.75^\circ$ grid covering the entire globe, but is available at a variety of resolutions. For this study, we use the $1^\circ \times 1^\circ$ grid to match the $1^\circ \times 1^\circ$ grids of the CERES and MODIS datasets (see below for details). We use the monthly means of daily means for each variable. Haimberger et al. (2001) show that the mass fluxes in ERA-Interim are unreliable and considered spurious, and, therefore, we remove their effect on energy transports following the methodology of Chiodo and Haimberger (2010) [see additionally, Mayer and Haimberger (2012)]. We examine the robustness of our results to these errors in section 4 and find that our conclusions remain unchanged.

For the radiative fluxes, we make use of CERES-EBAF data [see Wielicki et al. (1996, 1998) for a description of the CERES instrument and algorithm]. We make use of both CERES EBAF_Ed2.8 and CERES EBAF-Surface_Ed2.8 (see Loeb et al. 2009; Kato et al. 2013, respectively). The CERES data are on a $1^\circ \times 1^\circ$ grid. Despite the resolution being the same, the CERES data are on the grid centers (0.5°, 1.5°, etc.) while the ERA-Interim data are on the grid edges (0°, 1°, etc.). We regrid the CERES data onto the ERA-Interim grid so that the data are collocated. Again, we make use of

monthly averages for the top-of-the-atmosphere and surface fluxes.

Regional error estimates are 4 W m^{-2} for TOA shortwave (SW) fluxes, 5 W m^{-2} for longwave (LW) fluxes, 2.6 W m^{-2} for clear-sky SW fluxes, and 3.6 W m^{-2} for clear-sky LW fluxes (data quality summary). Over the March 2000–June 2002 period when only *Terra* was carrying the CERES instruments, the regional error for the TOA SW fluxes was slightly higher at 5 W m^{-2} . The surface fluxes for CERES have larger errors associated with the higher uncertainties inherent to the process of generating surface fluxes from spaceborne measuring systems. The errors are up to 11 W m^{-2} for upwelling and downwelling SW fluxes, 13 W m^{-2} for upwelling LW fluxes, and 12 W m^{-2} for downwelling LW fluxes.

To calculate errors for cloud radiative effects, we must combine errors from the individual sources. This is done as the square root of the sum of the squares, assuming the errors are uncorrelated. For example, the error in the CRE is $(4^2 + 5^2 + 2.6^2 + 3.6^2)^{1/2} = 8 \text{ W m}^{-2}$. Similarly, we calculate errors for SWCRE and LWCRE as 5 and 6 W m^{-2} , respectively. We are also interested in the atmospheric and surface cloud radiative effect (ACRE and SCRE, respectively). Similar to the TOA CRE calculated above, the error on the SCRE is $(11^2 + 11^2 + 13^2 + 12^2)^{1/2} = 24 \text{ W m}^{-2}$. Likewise, the error on the ACRE is $(8^2 + 24^2)^{1/2} = 25 \text{ W m}^{-2}$. The errors for ACRE are large, similar to those for AHT. However, ACRE is largely dictated by LWCRE (Ramanathan 1987; Slingo and Slingo 1988; Ramanathan et al. 1989; Tian et al. 2001). The actual errors in ACRE are likely to follow those of the LWCRE, which are only 6 W m^{-2} , and thus we do not expect the large error estimate for ACRE calculated here to alter our conclusions.

We investigate the western Pacific warm pool (10°S–10°N, 150°E–180°). We use CERES data from March 2000 through May 2014. The ERA-Interim dataset runs from 1979 to the present, but we use just the March 2000 through May 2014 period to be consistent with CERES. For comparison to the warm pool, we also investigate several other regions: the whole tropics (10°S–10°N, over all longitudes), the Atlantic Ocean (10°S–10°N, 60°W–0°), the Indian Ocean (10°S–10°N, 40°–100°E), and the eastern Pacific ITCZ (5°–15°N, 150°–100°W). For all regions, we consider only grid boxes that are over ocean. The seasonal cycle is removed from both the ERA-Interim and CERES-EBAF data so that the relationships shown in the results and discussion section are not simply due to the seasonal cycle. We have also performed the same analyses with the seasonal cycle included and find it does not alter our conclusions (not shown).

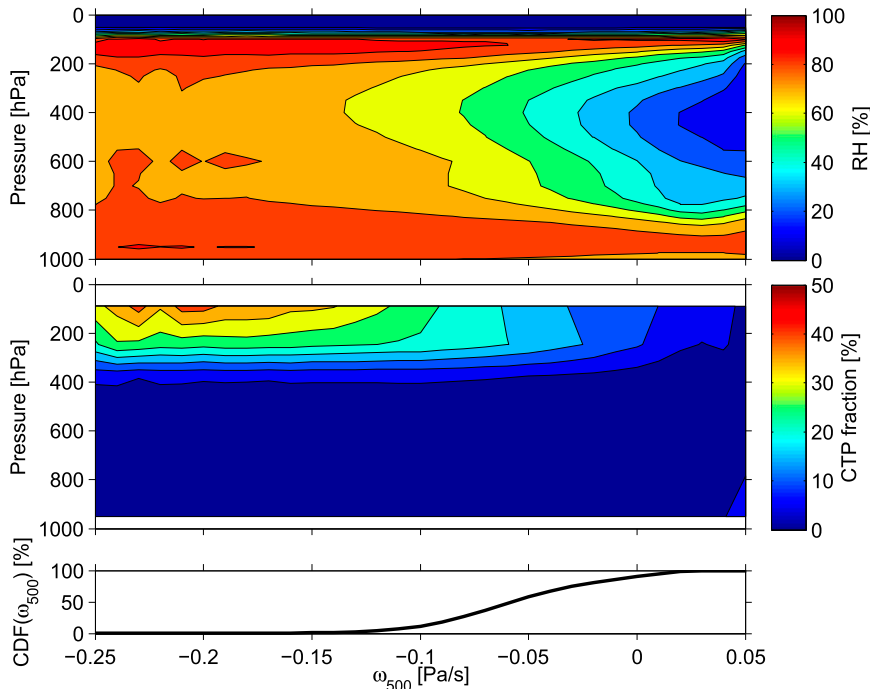


FIG. 1. (top) Relative humidity (%) as a function of pressure binned by ω_{500} for the warm pool region. Each bin has a width of 0.01 Pa s^{-1} . (middle) As in (top), but for MODIS-retrieved cloud-top pressure frequency. (bottom) Cumulative distribution function of ω_{500} .

It is important to consider the effect convection has on the clear-sky radiative cooling profile by changing the vertical distribution of water vapor. We expect that the AHT is related to the net change in radiative heating due to convection, and hence, the combined cloud and water vapor effect. We define the AMRE to be the difference between the actual clear-sky radiative heating (Rclr) and a baseline “nonconvective” clear-sky radiative heating profile. Since the goal is to analyze the effect of convection on the radiation budget, we use vertical velocity as a means of discriminating when convection is active. Therefore, the “nonconvective baseline” is calculated as the average radiative cooling for all points where $\omega_{500} > 0$. We select the $\omega_{500} > 0$ cutoff because there are very few clouds and the middle troposphere tends to be dry (see Fig. 1). The transition from a moist, cloudy atmosphere to a dry, cloud-free atmosphere is smooth in the warm pool, but the cutoff is more distinct across the whole of the tropics and occurs at $\omega_{500} = 0$ (not shown).

While the baseline criterion is the same across regions, the radiative cooling value calculated for that baseline is specific to each region. Thus, for analyses over regions outside the warm pool, the baseline is recalculated for each region of interest (the differences between regions are all less than 5 W m^{-2}). In the warm pool, the baseline Rclr is -132 W m^{-2} . The atmospheric moisture radiative

effect is reflected in changes in the top-of-the-atmosphere clear-sky radiative fluxes (mostly the outgoing long-wave radiation) and there is very little sensitivity of the surface clear-sky radiative fluxes to ω_{500} (not shown). We term the combined effect of ACRE and AMRE as ACoRE.

We have also investigated the impact of SST on Rclr and its subsequent influence on the baseline for the AMRE calculation. Radiative cooling increases with temperature, assuming constant specific humidity and all other atmospheric constituents. The baseline Rclr used for AMRE does have a SST dependence; however, the radiative cooling weakens as temperature increases, such that the impact of increasing water vapor far outweighs any temperature influence.

We use the MODIS histogram of cloud frequency binned by cloud optical thickness and cloud-top pressure. These MODIS data are available from July 2002 through the present as monthly averages on a $1^\circ \times 1^\circ$ grid. Like the CERES data, the MODIS data are on grid centers (0.5° , 1.5° , etc.); we regrid the MODIS data onto ERA-Interim grid so that the data are collocated. Because the MODIS data do not cover March 2000–June 2002, for the principal component analysis section of this paper, we only use data from July 2002 to May 2014 (the overlap period for all three datasets: ERA-Interim, CERES, and MODIS). The results derived from the

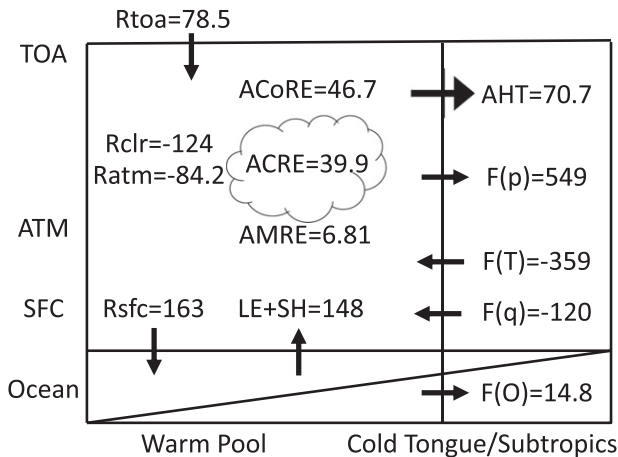


FIG. 2. Mean values over warm pool region (10°S – 10°N , 150°E – 180°) for radiative and turbulent fluxes, energy transport terms, and radiative heating (all in W m^{-2}). AHT is the net divergence of moist static energy, $F(p)$ is the divergence of potential energy, $F(T)$ is the divergence of sensible energy, $F(q)$ is the divergence of latent energy, and $F(O)$ is the divergence of energy through the ocean. ACoRE, ACRE, and AMRE are detailed in the text. Rclr and Ratm are the integrated clear-sky radiative cooling and integrated radiative heating, respectively. Rtoa and Rsfc are the top-of-the-atmosphere and surface radiative fluxes, respectively. LE + SH is the combined latent and sensible heat fluxes at the surface.

ERA-Interim and CERES datasets alone are not sensitive to the change in record length.

The terms that are of most interest to us are the atmospheric radiative cooling (both all sky and clear sky), the top-of-the-atmosphere and surface radiative fluxes, the atmospheric cloud radiative effect, the atmospheric moisture radiative effect, the atmospheric convective radiative effect, the surface turbulent heat fluxes, and the divergence of total energy transport. The atmospheric radiative cooling, TOA and SFC radiative fluxes, and atmospheric cloud radiative effect are all taken directly from the CERES monthly data. The atmospheric moisture radiative effect and atmospheric convective radiative effect are computed as described above, and are calculated using a combination of CERES and ERA-Interim monthly data. The surface turbulent fluxes and divergence of total energy transport are directly taken from the ERA-Interim monthly data.

3. Results and discussion

We begin by calculating the average values for the fluxes and heat transport terms for the warm pool region. We present the results in a similar fashion to Fig. 7 of Tian et al. (2001) (see Fig. 2). The values in Fig. 2 differ from those of Tian et al. (2001) owing to measurement changes, use of reanalysis, and length of

record differences. As noted in section 2, all of the radiative flux-dependent variables (Rtoa, Rclr, Ratm, Rsfc, and ACRE) are calculated using CERES data, ACoRE and AMRE are calculated using a combination of CERES and ERA-Interim data, while the rest of the values in Fig. 2 are from ERA-Interim data. The top-of-the-atmosphere net radiative flux (Rtoa) is roughly 30 W m^{-2} less in our climatology than that reported by Tian et al. (2001), while the surface net radiative flux (Rsfc) is roughly 15 W m^{-2} greater. These combine to make the net radiative cooling roughly 45 W m^{-2} stronger in our climatology than that reported by Tian et al. (2001).

ACRE is calculated as the difference between the clear-sky net radiative heating and the all-sky net radiative heating. Tian et al. (2001) use the Earth Radiation Budget Experiment (ERBE) for the top-of-the-atmosphere fluxes, and they use Tropical Ocean and Global Atmosphere Coupled Ocean–Atmosphere Response Experiment (TOGA COARE) and Central Equatorial Pacific Experiment (CEPEX) observations for the surface fluxes. For the clear-sky radiative heating, Tian et al. (2001) use the tropical profile from Dopplnick (1979). The radiative heating profiles calculated in Dopplnick (1979), however, contain clouds (see Dopplnick 1972 for details). Therefore, the ACRE estimate provided by Tian et al. (2001) is likely an underestimate, yet it is still greater than that calculated from the CERES data. The roughly 30 W m^{-2} difference between our value and that of Tian et al. (2001) results from the 45 W m^{-2} difference in all-sky radiative cooling being offset by the 15 W m^{-2} difference in clear-sky radiative cooling.

The divergence of total energy transport (AHT) is only about 10 W m^{-2} less in our climatology than the value reported by Tian et al. (2001), despite larger differences between the component terms: internal, potential, and latent. Our value for the total surface turbulent heat fluxes is about 30 W m^{-2} larger than that of Tian et al. (2001), which, when combined with the difference in surface radiative fluxes, makes our oceanic energy divergence about 15 W m^{-2} weaker than the value given by Tian et al. (2001).

The values that are of most interest for this study are the ACoRE and the net energy divergence (or AHT). Over the 14-yr record and within the warm pool, the ACoRE balances 66% of the total AHT, with the ACRE balancing 56% of the AHT and the AMRE balancing 9.6% of the AHT. The ratio of ACRE to AHT given in Fig. 2 is smaller than that calculated by Tian et al. (2001, roughly 88% in their data). We offset some of that difference with the inclusion of the radiative heating due to moisture. The ACoRE and the AHT vary

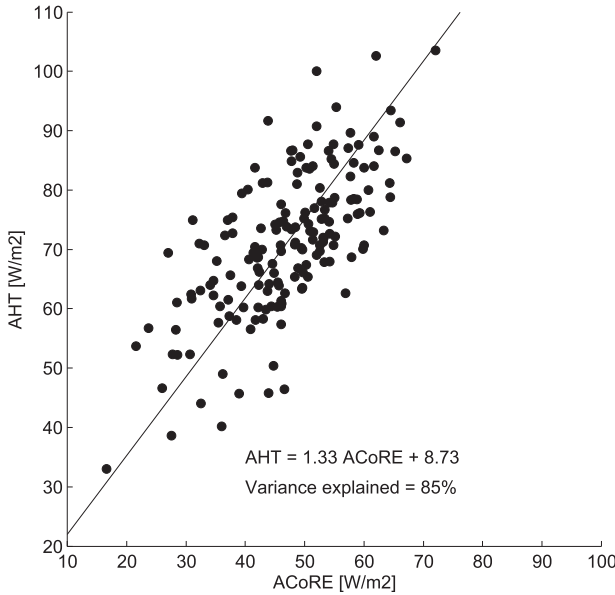


FIG. 3. ACoRE (ACRE + AMRE) vs total energy divergence (AHT) over the warm pool. Each point represents one monthly averaged value over the entire warm pool region (10°S–10°N, 150°E–180°). The line is the linear fit to the data obtained by principal component analysis (in this case, 85% of the variance is explained by this line).

from month to month throughout the 14-yr time period. The variations, however, are not random, but are well correlated (significant at the 95% level; see Fig. 3).

Since we do not know either ACoRE or AHT with absolute certainty, we use EOF analysis to minimize the perpendicular distance of the data from the linear fit instead of ordinary least squares. Figure 3 shows that best fit line is roughly a 1:1 line with a y intercept of 8.73 W m⁻² (meaning even when ACoRE = 0, there is

still heat transport of nearly 9 W m⁻²). We can compare this y-intercept value with the predicted value of AHT when ACoRE = 0. By energy conservation, the heat transport must equal the difference in surface turbulent fluxes and the radiative cooling of the atmosphere. We can break the radiative cooling of the atmosphere into a nonconvective radiative cooling amount similar to our construction of AMRE (see above) and ACoRE. Written out this gives

$$AHT = ACoRE + (LE + SH) - R_0, \quad (1)$$

where LE is the surface latent heat flux, SH is the surface sensible heat flux, and R₀ is the nonconvective radiative cooling of the atmosphere. From Eq. (1), when ACoRE = 0, AHT = (LE + SH) - R₀. Over the warm pool, LE + SH = 148 W m⁻² (see Fig. 2) and R₀ = 132 W m⁻² (equivalent to R_{clr} - AMRE). Thus, when ACoRE = 0, we would expect AHT = 16 W m⁻², close to the 8.73 W m⁻² y intercept for the EOF line in Fig. 3, considering the uncertainty on the surface radiative flux estimates.

We next bin ACoRE (and its components: ACRE and AMRE) and AHT by sea surface temperature (see Fig. 4, left panel) and vertical velocity along the 500-hPa surface (see Fig. 4, right panel). At SSTs warmer than about 301 K, ACoRE and AHT rise together at nearly a 1:1 rate with increasing SST. Most of the increase in ACoRE comes from increases in the clouds (ACRE). Over the same range of SSTs, we see that the surface turbulent fluxes (latent and sensible heat) do not vary much (within ±10 W m⁻² of 150 W m⁻²). By energy conservation, changes in ACoRE, AHT, and surface turbulent fluxes (LE + SH) must balance one another, so it is guaranteed that if ACoRE and AHT increase at

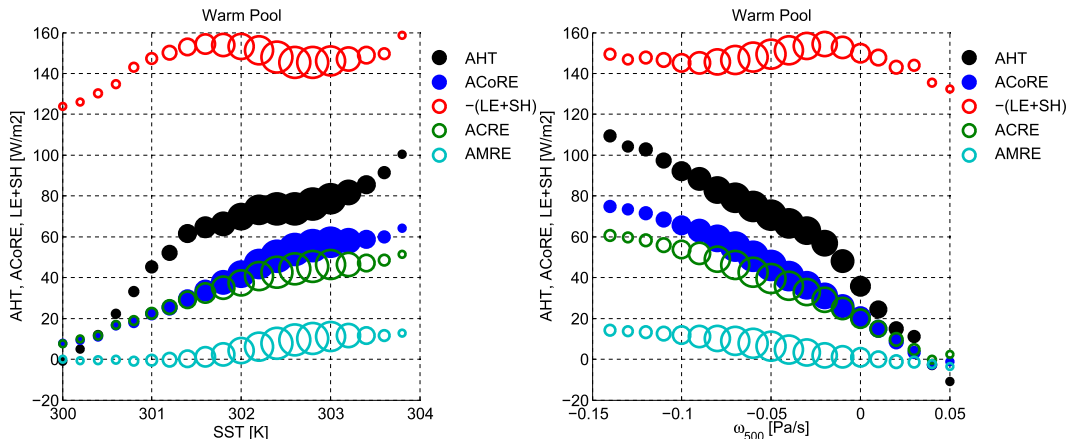


FIG. 4. (left) ACoRE, AHT, ACRE, AMRE, and surface turbulent fluxes [-(LE + SH)] binned by SST (bin intervals are 0.2 K). The size of the circle is scaled by the frequency of occurrence of that SST in the warm pool region. (right) As in (left), but binned by ω₅₀₀ (bin intervals are 0.01 Pa s⁻¹).

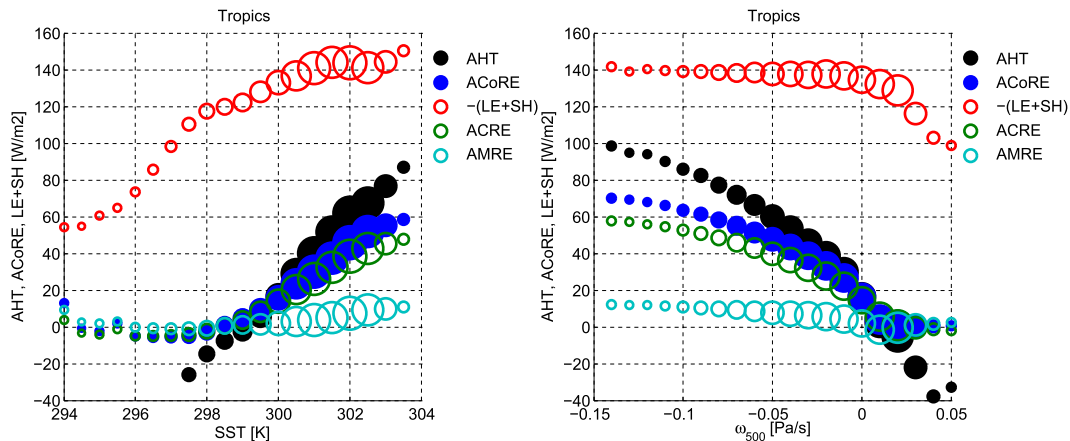


FIG. 5. As in Fig. 4, but only over the entire tropics ($10^{\circ}S$ – $10^{\circ}N$, over all longitudes); ocean grid cells only. The range of SSTs for the tropics is larger than that used for binning the data over the warm pool.

exactly the same rate with increasing SST, then $LE + SH$ must be approximately constant. When we bin the data by vertical velocity on the 500-hPa surface (ω_{500}), the relationship between ACoRE and AHT is similar to that when the data are binned by SST. As the pressure velocity decreases (stronger upward motion), ACoRE and AHT increase together, while the surface turbulent fluxes decrease slightly. Again, most of the increase in ACoRE comes from an increase in ACRE. The relationships between ACoRE and AHT can be seen elsewhere in the tropics as well. We bin the tropical average ACoRE and AHT (not including regions over land) by SST and ω_{500} (see Fig. 5). Figure 5 shows that the ACoRE and AHT relationship shares many features with the warm pool (though spanning a larger range of SSTs).

We investigate other convective regions of the tropics (see Table 2) and find similar structures in the ACoRE and AHT relationship in these regions to those found in the warm pool (not shown). Table 2 shows the amount of AHT balanced by ACoRE for the warm pool, tropical average, the Atlantic, the Indian Ocean, the eastern Pacific ITCZ, and the broader western Pacific regions. We note that the percentage of AHT balanced by

ACoRE is roughly the same over convective regions at 66%–87%. The breakdown of ACoRE into ACRE and AMRE is also roughly the same over convective regions (56%–74% ACRE and 5.5%–13% AMRE), suggesting that this is a robust feature of tropical convection.

We next shift focus to the TOA. Figure 6 shows the net TOA radiative fluxes (R_{net}) and the TOA CRE. As expected, increases in convection increase both the shortwave cloud radiative effect (SWCRE) and the longwave cloud radiative effect (LWCRE) as seen when binned by either SST or ω_{500} . CRE, however, behaves differently depending on whether we bin by SST or ω_{500} . While CRE does not have any discernible relationship with the underlying SSTs over the warm pool, when binned by ω_{500} , CRE decreases for increasing ω_{500} (see Fig. 6). Increases in vertical velocity are indicative of increases in convection, which one would expect to result in increases in the magnitude of both SWCRE and LWCRE. We find, however, that SWCRE increases in magnitude more rapidly with ω_{500} than does LWCRE. We will explore this result in greater detail below. Figure 6 (right panel) shows that the decrease in CRE with increasing convection is balanced by an increase in AMRE such that R_{net} are unchanged. The insensitivity

TABLE 2. Average ACRE, AMRE, ACoRE, and AHT ($W m^{-2}$) for various regions in the tropics. The numbers in parentheses are the fraction of AHT balanced by ACRE, AMRE, or ACoRE. All regions range from $10^{\circ}S$ to $10^{\circ}N$ except for the eastern Pacific, which is 5° – $15^{\circ}N$. All averages are taken over ocean grid cells only.

	ACRE	AMRE	ACoRE	AHT
Warm pool ($150^{\circ}E$ – 180°)	39.9 (56%)	6.81 (9.6%)	46.7 (66%)	70.7
Tropics (all lon)	23.7 (74%)	4.28 (13%)	28.0 (87%)	32.2
Indian Ocean (40° – $100^{\circ}E$)	30.9 (62%)	4.55 (9.2%)	35.5 (71%)	49.6
Atlantic ($60^{\circ}W$ – 0°)	14.7 (60%)	2.62 (11%)	17.3 (71%)	24.3
Western Pacific ($120^{\circ}E$ – 180°)	40.3 (63%)	6.09 (9.6%)	46.4 (73%)	63.7
Eastern Pacific (150° – $100^{\circ}W$)	23.6 (66%)	1.97 (5.5%)	25.6 (71%)	35.9

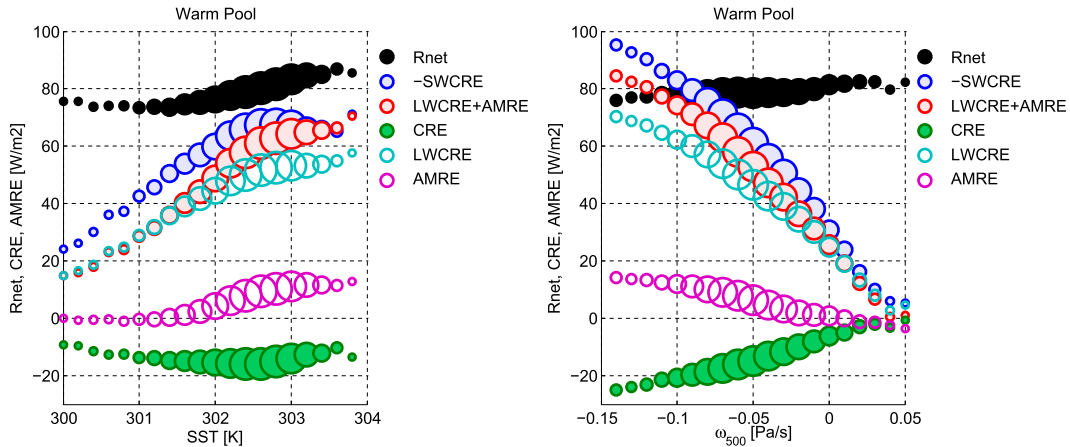


FIG. 6. (left) R_{net} , $-SWCRE$, $LWCRE + AMRE$, CRE , $LWCRE$, and $AMRE$ in the warm pool binned by SST (bin intervals are 0.2 K). The size of the circle is scaled by the frequency of occurrence of that SST in the warm pool region. (right) As in (left), but binned by ω_{500} (bin intervals are 0.01 Pa s^{-1}).

between circulation strength and top-of-the-atmosphere fluxes was shown by [Clement and Soden \(2005\)](#), though they suggested the insensitivity was a cloud-driven effect while we show that water vapor is also important.

We perform principal component analysis on MODIS data to investigate the behavior of the CRE over the warm pool. [Figure 7](#) shows the mean histogram of MODIS-retrieved cloud optical thickness versus cloud-top pressure over the warm pool (for brevity, we refer to this as the MODIS histogram). As expected, high clouds (cloud-top pressure < 440 hPa) are the most common cloud type observed by MODIS over the warm pool.

We calculate the EOFs for the MODIS histogram at all points within the warm pool and for all months (see [Fig. 8](#)). The first three EOFs show the three modes of variability that explain the largest fraction of the variance in the MODIS histogram. The first EOF (53% variance explained) is an increase in high clouds across a range of optical depths and cloud-top pressures similar to the mean MODIS histogram structure. The second EOF (20% of variance explained) is a shift from optically thin to optically thick clouds. The third EOF (11% of variance explained) is a vertical shift of the high clouds in pressure coordinates. We can think of these three EOFs as cloud amount, cloud optical thickness, and cloud-top height, respectively. We then calculate the principal components for each EOF to get the amplitudes of each pattern across all points within the warm pool and all months of the MODIS record (see [Fig. 9](#)).

As the SSTs increase, PC1 and PC3 increase, while PC2 decreases. As ω_{500} decreases, all three principal components increase, with PC1 showing the largest change. We use the net cloud forcing histograms from

[Hartmann et al. \(2001, their Fig. 5a\)](#) to get a measure of how the cloud radiative effect changes depending on the amplitude of each EOF pattern. The change in top-of-the-atmosphere net cloud radiative effect for a one standard deviation increase is -3.78 W m^{-2} for EOF1, -6.63 W m^{-2} for EOF2, and $+1.36 \text{ W m}^{-2}$ for EOF3. The cloud amount change associated with one standard deviation of the principal component of EOF1 is much more than the cloud amount changes associated with one standard deviation of the principal components of EOF2 and EOF3. If we were to normalize the three leading EOFs such that the increases in clouds are all 10%, then the changes in CRE would be -2.56 W m^{-2} for EOF1, -14.0 W m^{-2} for EOF2, and $+5.20 \text{ W m}^{-2}$ for

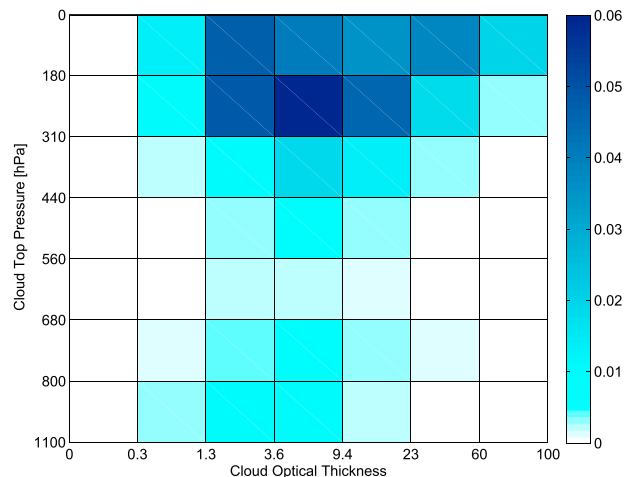


FIG. 7. MODIS frequency histogram of cloud optical thickness vs cloud-top pressure. The data are monthly mean values over the warm pool region defined above.

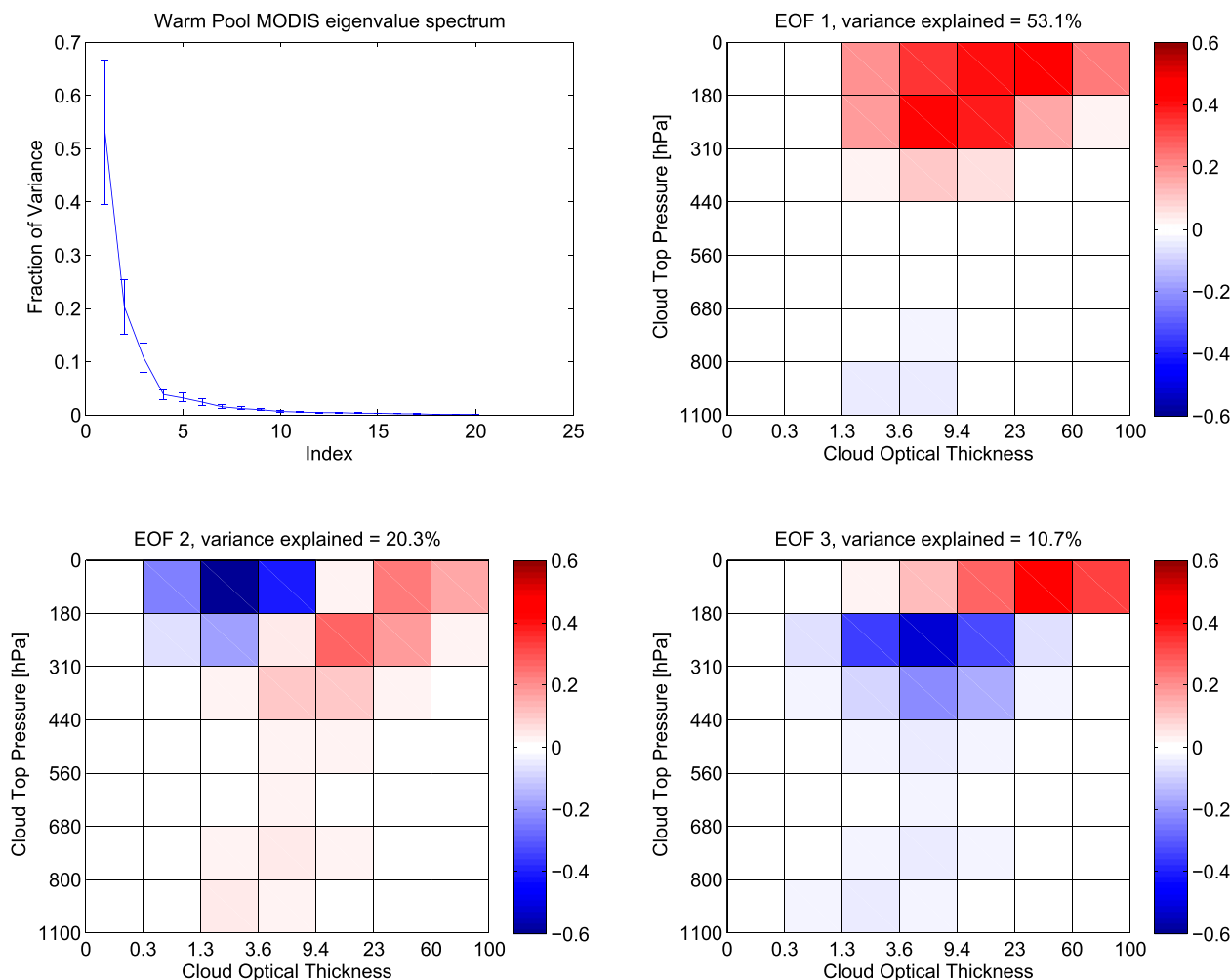


FIG. 8. (top left) Eigenvalue spectrum for EOF analysis of MODIS cloud optical thickness vs cloud-top pressure histogram. The first three EOFs of the MODIS histogram: (top right) EOF1, (bottom left) EOF2, and (bottom right) EOF3. The change in top-of-the-atmosphere net cloud radiative effect for a one standard deviation increase in each of the above EOFs is -3.78 , -6.63 , and $+1.36 \text{ W m}^{-2}$, respectively.

EOF3. The previous calculation reveals that changes in cloud optical thickness or cloud-top height have the potential to alter the CRE much more than changes in overall cloud amount, but do not vary enough over the warm pool to be the dominant factor. Cloud amount (EOF1) has a weak negative effect on CRE.

We bin the CRE changes explained by each principal component against SST and ω_{500} as before (see Fig. 10). Figure 10 shows that the first three PCs of the MODIS histogram do a good job of representing the total change in CRE from its mean value due to changes in SST or ω_{500} (cf. Figs. 10 and 6). The overall change in CRE with increasing SST is small, as we saw before, while increasing ω_{500} leads to increases in CRE, again, as seen above. Further, Fig. 10 shows that the small change in CRE with increasing SST is largely due to compensation

between the effects of different EOFs. As SST increases, the effect of cloud amount increases (PC1) is compensated by both cloud optical thickness decreases (PC2) and cloud-top height increases (PC3). As SSTs increase, the cloud amount increases and the ΔCRE becomes more negative (at -3.78 W m^{-2} per standard deviation increase). At the same time, however, increasing SSTs are associated with a shift toward optically thinner clouds providing a positive change in ΔCRE , while increasing SSTs favor higher cloud tops (also increasing ΔCRE). Since the magnitudes of these changes are comparable, little net change in CRE results from changes in SST over the warm pool. As for changes in ω_{500} , much of the variability is due to changes in cloud amount (PC1), with cloud optical thickness being a secondary factor, and cloud-top height playing virtually no role at all. As upward

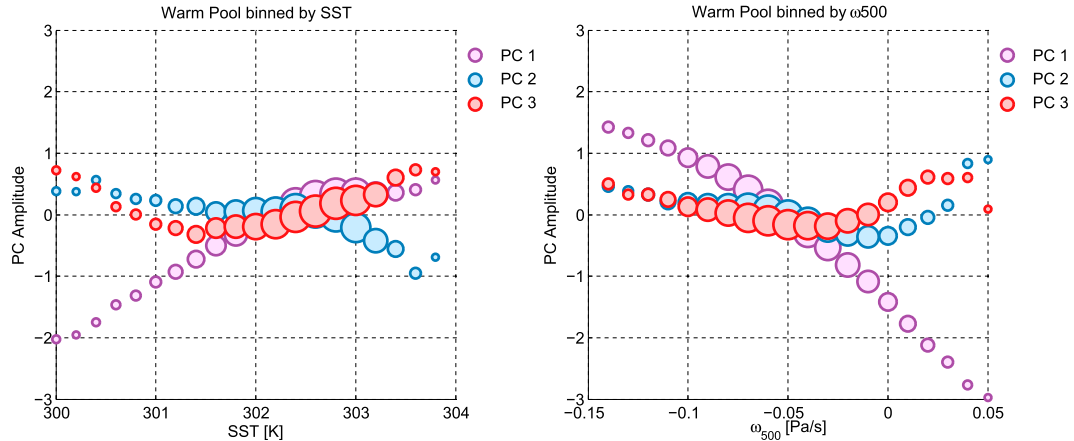


FIG. 9. Principal components of EOFs presented in Fig. 8 binned by (left) SST and (right) ω_{500} . PC1, PC2, and PC3 represent changes in cloud amount, cloud optical thickness, and cloud-top height, respectively.

vertical velocities increase (more convection), the amount of clouds increase and their optical thickness distribution shifts toward thicker clouds. Since both of these features act to drive Δ CRE in the same direction, there is no cancellation effect, and the CRE becomes more negative as upward vertical velocity increases.

Figure 11 shows that the atmospheric heat transport responds more strongly to PC1 (cloud amount) than either PC2 or PC3 (cloud optical thickness and cloud-top height, respectively). Changes from optically thin to optically thick clouds (PC2) have virtually no impact on the AHT, ACoRE, ACRE, or AMRE. Changes in cloud-top height (PC3) have a peculiar behavior with a minimum in AHT and ACRE near an amplitude of one for PC3. The relationship between cloud amount (PC1) and AHT is very similar to the relationship between ω_{500} and AHT, reaffirming that the influence of vertical velocity

on AHT and ACoRE is driven by changes in cloud amount and not cloud structure.

4. Additional sensitivity tests

As noted in section 2, several sensitivity tests were performed to test the robustness of our conclusions. In short, the structures in the relationship between ACoRE and AHT are robust. The relationships have virtually no change whether we use an “indirect” or “direct” calculation of AHT, whether we use daily instead of monthly data, or whether we use the ERA-Interim radiative fluxes in place of CERES fluxes. Note that the indirect calculation of AHT uses the top-of-the-atmosphere and surface fluxes to determine the net energy divergence while the direct calculation uses the actual divergence of total energy.

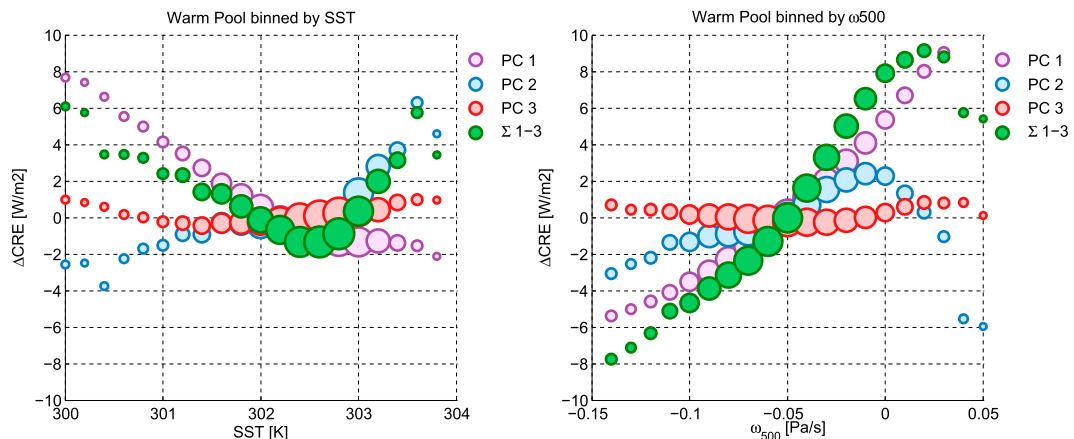


FIG. 10. Change in CRE due to variability in cloud amount, cloud optical thickness, and cloud-top height (PC1, PC2, and PC3, respectively) as binned by (left) SST and (right) ω_{500} . The green dots represent the sum of the change in CRE due to the first three principal components.

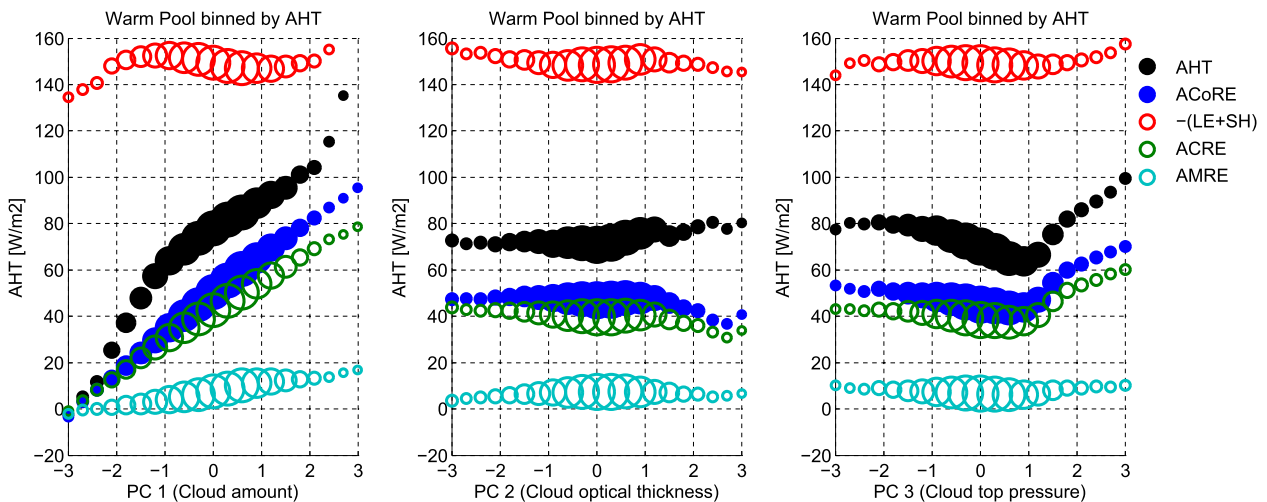


FIG. 11. As in Fig. 4, but only AHT, ACoRE (ACRE + AMRE), $-(LE+SH)$, ACRE, and AMRE are binned by the amplitude of (left) PC1, (center) PC2, and (right) PC3.

We begin with errors in the AHT. To investigate whether these errors may confound our results, we compare the AHT output from ERA-Interim (the direct AHT calculation) with that computed using the top-of-the-atmosphere and surface fluxes (the indirect AHT calculation). The structural relationship between ACoRE and AHT is not changed when switching between the direct and indirect AHT calculations (not shown). The magnitude of the average AHT over the warm pool drops by about 6.7 W m^{-2} when using the indirect calculation compared to the direct calculation.

When using ERA-Interim radiative fluxes, the major difference comes from ACRE, with the ERA-Interim estimate being smaller than that of CERES. ERA-Interim-derived ACoRE averaged over the warm pool is 41.8 W m^{-2} (59% of AHT), with $ACRE = 33.1 \text{ W m}^{-2}$ (47% of AHT) and $AMRE = 8.67 \text{ W m}^{-2}$ (12% of AHT). ACRE is smaller in the ERA-Interim estimate than the CERES estimate (-6.8 W m^{-2}). AMRE is larger in the ERA-Interim estimate than the CERES estimate ($+1.9 \text{ W m}^{-2}$). The ACRE decrease is more than twice that of the AMRE increase, such that ACoRE is smaller when calculated by ERA-Interim instead of CERES (-4.9 W m^{-2}). As expected from the ACRE results above, there are shifts in the magnitudes of the cloud radiative effects and net radiative fluxes, but the conclusion are unchanged (not shown).

We have tested whether our conclusions are sensitive to the monthly averaging time scale, most notably the atmospheric heat transport. We downloaded one year of daily ERA-Interim data from the time period used in the study. For this test, we make use of the ERA-Interim radiative fluxes, since they behave similarly to the

CERES-EBAF fluxes as noted above. Year 2013 was chosen as it is the last full calendar year in our time period. The patterns in AHT, ACoRE, etc. are the same for both the daily and monthly data (not shown).

5. Conclusions

The analysis and data presented here confirm that the atmospheric cloud radiative effect (ACRE) contributes to enhanced atmospheric heat transport (AHT) in the tropics as was shown by previous studies (e.g., Sherwood et al. 1994; Sohn 1999; Bergman and Hendon 2000a; Tian et al. 2001; Tian and Ramanathan 2002). Additionally, we find the atmospheric moisture radiative effect (AMRE) is important and acts in the same way as the cloud radiative heating, and we refer to their combined effect as the atmospheric convective radiative effect (ACoRE). Atmospheric radiative heating due to increases in clouds and water vapor balances 66% of the net energy divergence out of the tropical warm pool atmosphere (10°S – 10°N , 150°E – 180°) during our 14-yr time period. Tian et al. (2001) found ACRE balanced 88% of AHT during the TOGA COARE and CEPEX period. Month to month changes in the net energy divergence and the radiative heating from clouds and water vapor covary at roughly a 1:1 rate, shown by a linear fit, which explains 85% of the variance. The covariations in the net horizontal energy divergence and the atmospheric radiative heating from clouds and water vapor show consistent relationships with sea surface temperature and vertical velocity. Increases in sea surface temperature lead to equal increases in both net horizontal energy divergence and atmospheric radiative

heating. The same is true for increases in upward vertical velocity. These results hold in different regions of the tropics as well, with the proportion of net horizontal energy divergence balanced by atmospheric radiative heating from clouds and water vapor ranging from 66% to 87%.

In the warm pool, the cloud radiative effect (CRE) at the top of the atmosphere is insensitive to sea surface temperature changes, owing to compensation between increases in all types of high clouds and a shift toward higher, thinner clouds. The longwave and shortwave cloud radiative effects (LWCRE and SWCRE, respectively) both increase in magnitude with increasing sea surface temperature in good agreement with Bony et al. (1997). Additionally, the net radiative fluxes at the top of the atmosphere are insensitive to changes in vertical velocity (in agreement with Clement and Soden 2005). Unlike Clement and Soden (2005), we find that the insensitivity of top-of-the-atmosphere fluxes to vertical velocity is due to compensating changes in the CRE and AMRE. Negative anomalies in CRE are balanced by enhanced water vapor greenhouse effect. The decrease in CRE with increasing vertical velocity agrees with results from Yuan et al. (2008). The introduction of AMRE, however, is new to this study. The insensitivity of top-of-the-atmosphere fluxes to circulation strength means horizontal transport of energy by the atmosphere can increase or decrease without any change in the top-of-the-atmosphere fluxes. If the atmosphere remains in steady state, then surface fluxes must compensate for the change in atmospheric heat transport. Increases in upward vertical velocity increase cloud amount as well, but also shift the cloud distribution toward more optically thick clouds, thus decreasing the cloud radiative effect. We have shown that cloud amount (EOF1) is the dominant mode of variability for the cloud systems and accounts for the majority of the month-to-month changes in both the net horizontal energy divergence out of the column and the atmospheric convective radiative effect. It is reasonable to expect cloud amount to be tied to the mass flux. Similarly, the amount of water vapor lofted into the upper troposphere should also be tied to the mass flux. The amount of water vapor lofted is responsible for determining the atmospheric moisture radiative effect. As noted above, the insensitivity of the top-of-the-atmosphere fluxes to circulation strength is only achieved by the cancellation between decreasing CRE and increasing AMRE. It is worth investigating the cause of this cancellation in future work. Additionally, it is important to ask whether the cancellation between changes in CRE and AMRE can be expected to continue in a warming climate. If not, strong feedbacks may arise due to the imbalance at the top of the atmosphere

that either enhance or dampen variability in the tropical circulation.

The work presented in this paper raises further questions related to the relationship between ACoRE and the net divergence of energy (AHT). For instance, do models reproduce the same ACoRE–AHT relationship seen above? If yes, is that relationship preserved through a warming climate? If the radiative effects of clouds are removed, do we see a drop off in AHT equivalent to the atmospheric cloud radiative effect? Does a slowdown of the tropical circulation in a warmer climate necessitate a reduction in cloud amount as is seen in the current climate? The answers to these questions will deepen our understanding of the relationship between the tropical circulation and the radiative heating due to clouds and water vapor.

Acknowledgments. The CERES EBAF data were obtained from the NASA Langley Research Center CERES ordering tool (<http://ceres.larc.nasa.gov/>). The ERA-Interim data were obtained from the ECMWF Data Server (<http://apps.ecmwf.int/datasets/data/interim-full-moda>). The MODIS data used in this study were acquired as part of the NASA's Earth-Sun System Division and archived and distributed by the MODIS Adaptive Processing System (MODAPS). These MODIS data were obtained from the LAADS FTP server (<ftp://ladsweb.nascom.nasa.gov/>). The authors also wish to thank our anonymous reviewers for their suggestions toward improving this manuscript. Funding for this work was provided by NSF Grant AGS-0960497.

REFERENCES

- Bergman, J. W., and H. H. Hendon, 2000a: Cloud radiative forcing of the low-latitude tropospheric circulation: Linear calculations. *J. Atmos. Sci.*, **57**, 2225–2245, doi:10.1175/1520-0469(2000)057<2225:CRFOTL>2.0.CO;2.
- , and —, 2000b: The impact of clouds on the seasonal cycle of radiative heating over the Pacific. *J. Atmos. Sci.*, **57**, 545–566, doi:10.1175/1520-0469(2000)057<0545:TIOCOT>2.0.CO;2.
- Bony, S., K.-M. Lau, and Y. C. Sud, 1997: Sea surface temperature and large-scale circulation influences on tropical greenhouse effect and cloud radiative forcing. *J. Climate*, **10**, 2055–2077, doi:10.1175/1520-0442(1997)010<2055:SSTALS>2.0.CO;2.
- , J.-L. Dufresne, H. Le Treut, J.-J. Morcrette, and C. Senior, 2004: On dynamic and thermodynamic components of cloud changes. *Climate Dyn.*, **22**, 71–86, doi:10.1007/s00382-003-0369-6.
- Cess, R. D., M. Zhang, B. A. Wielicki, D. F. Young, X.-L. Zhou, and Y. Nikitenko, 2001: The Influence of the 1998 El Niño upon cloud-radiative forcing over the Pacific warm pool. *J. Climate*, **14**, 2129–2137, doi:10.1175/1520-0442(2001)014<2129:TITOTEN>2.0.CO;2.
- Chiodo, G., and L. Haimberger, 2010: Interannual changes in mass consistent energy budgets from ERA-Interim and satellite data. *J. Geophys. Res.*, **115**, D02112, doi:10.1029/2009JD012049.

- Clement, A. C., and B. Soden, 2005: The sensitivity of the tropical-mean radiation budget. *J. Climate*, **18**, 3189–3203, doi:10.1175/JCLI3456.1.
- Dee, D. P., and Coauthors, 2011: The ERA-Interim reanalysis: Configuration and performance of the data assimilation system. *Quart. J. Roy. Meteor. Soc.*, **137**, 553–597, doi:10.1002/qj.828.
- Dopplack, T. G., 1972: Radiative heating of the global atmosphere. *J. Atmos. Sci.*, **29**, 1278–1294, doi:10.1175/1520-0469(1972)029<1278:RHOTGA>2.0.CO;2.
- , 1979: Radiative heating of the global atmosphere: Corrigendum. *J. Atmos. Sci.*, **36**, 1812–1817, doi:10.1175/1520-0469(1979)036<1812:RHOTGA>2.0.CO;2.
- Franklin, C. N., Z. Sun, D. Bi, M. Dix, H. Yan, and A. Bodas-Salcedo, 2013: Evaluation of clouds in ACCESS using the satellite simulator package COSP: Regime-sorted tropical cloud properties. *J. Geophys. Res. Atmos.*, **118**, 6663–6679, doi:10.1002/jgrd.50496.
- Haimberger, L., B. Ahrens, F. Hamelbeck, and M. Hantel, 2001: Impact of time sampling on atmospheric energy budget residuals. *Meteor. Atmos. Phys.*, **77**, 167–184, doi:10.1007/s007030170025.
- Harrison, E. F., P. Minnis, B. R. Barkstrom, V. Ramanathan, R. D. Cess, and G. G. Gibson, 1990: Seasonal variation of cloud radiative forcing derived from the Earth Radiation Budget Experiment. *J. Geophys. Res.*, **95**, 18 687–18 703, doi:10.1029/JD095iD11p18687.
- Harshvardhan, D. A. Randall, and D. A. Dazlich, 1990: Relationship between the longwave cloud radiative forcing at the surface and the top of the atmosphere. *J. Climate*, **3**, 1435–1443, doi:10.1175/1520-0442(1990)003<1435:RBTLCR>2.0.CO;2.
- Hartmann, D. L., L. A. Moy, and Q. Fu, 2001: Tropical convection and the energy balance at the top of the atmosphere. *J. Climate*, **14**, 4495–4511, doi:10.1175/1520-0442(2001)014<4495:TCATEB>2.0.CO;2.
- Hwang, Y.-T., and D. M. W. Frierson, 2010: Increasing atmospheric poleward energy transport with global warming. *Geophys. Res. Lett.*, **37**, L24807, doi:10.1029/2010GL045440.
- Kato, S., N. G. Loeb, F. G. Rose, D. R. Doelling, D. A. Rutan, T. E. Caldwell, L. Yu, and R. A. Weller, 2013: Surface irradiances consistent with CERES-derived top-of-atmosphere shortwave and longwave irradiances. *J. Climate*, **26**, 2719–2740, doi:10.1175/JCLI-D-12-00436.1.
- Kiehl, J. T., 1994: On the observed near cancellation between longwave and shortwave cloud forcing in tropical regions. *J. Climate*, **7**, 559–565, doi:10.1175/1520-0442(1994)007<0559:OTONCB>2.0.CO;2.
- , and V. Ramanathan, 1990: Comparison of cloud forcing derived from the Earth Radiation Budget Experiment with that simulated by the NCAR Community Climate Model. *J. Geophys. Res.*, **95**, 11 679–11 698, doi:10.1029/JD095iD08p11679.
- Lee, S., and C. Yoo, 2014: On the causal relationship between poleward heat flux and the equator-to-pole temperature gradient: A cautionary tale. *J. Climate*, **27**, 6519–6525, doi:10.1175/JCLI-D-14-00236.1.
- Loeb, N. G., B. A. Wielicki, D. R. Doelling, G. L. Smith, D. F. Keyes, S. Kato, N. Manalo-Smith, and T. Wong, 2009: Toward optimal closure of the earth's top-of-atmosphere radiation budget. *J. Climate*, **22**, 748–766, doi:10.1175/2008JCLI2637.1.
- Mayer, M., and L. Haimberger, 2012: Poleward atmospheric energy transports and their variability as evaluated from ECMWF reanalysis data. *J. Climate*, **25**, 734–752, doi:10.1175/JCLI-D-11-00202.1.
- Platnick, S., M. D. King, S. A. Ackerman, W. P. Menzel, B. A. Baum, J. C. Riedi, and R. A. Frey, 2003: The MODIS cloud products: Algorithms and examples from Terra. *IEEE Trans. Geosci. Remote Sens.*, **41**, 459–473, doi:10.1109/TGRS.2002.808301.
- Ramanathan, V., 1987: The role of earth radiation budget studies in climate and general circulation research. *J. Geophys. Res.*, **92**, 4075–4095, doi:10.1029/JD092iD04p04075.
- , R. Cess, E. Harrison, P. Minnis, B. Barkstrom, E. Ahmad, and D. Hartmann, 1989: Cloud-radiative forcing and climate: Results from the Earth Radiation Budget Experiment. *Science*, **243**, 57–63, doi:10.1126/science.243.4887.57.
- Randall, D. A., D. A. Dazlich, and T. G. Corsetti, 1989: Interactions among radiation, convection, and large-scale dynamics in a general circulation model. *J. Atmos. Sci.*, **46**, 1943–1970, doi:10.1175/1520-0469(1989)046<1943:IARCAL>2.0.CO;2.
- Sherwood, S. C., V. Ramanathan, T. P. Barnett, M. K. Tyree, and E. Roeckner, 1994: Response of an atmospheric general circulation model to radiative forcing of tropical clouds. *J. Geophys. Res.*, **99**, 20 829–20 845, doi:10.1029/94JD01632.
- Slingo, A., and J. M. Slingo, 1988: The response of a general circulation model to cloud longwave radiative forcing. I: Introduction and initial experiments. *Quart. J. Roy. Meteor. Soc.*, **114**, 1027–1062, doi:10.1002/qj.49711448209.
- Slingo, J. M., and A. Slingo, 1991: The response of a general circulation model to cloud longwave radiative forcing. II: Further studies. *Quart. J. Roy. Meteor. Soc.*, **117**, 333–364, doi:10.1002/qj.49711749805.
- Sohn, B.-J., 1999: Cloud-induced infrared radiative heating and its implications for large-scale tropical circulations. *J. Atmos. Sci.*, **56**, 2657–2672, doi:10.1175/1520-0469(1999)056<2657:CIIRHA>2.0.CO;2.
- Stuhlmanner, R., and G. L. Smith, 1988a: A study of cloud-generated radiative heating and its generation of available potential energy. Part I: Theoretical background. *J. Atmos. Sci.*, **45**, 3911–3927, doi:10.1175/1520-0469(1988)045<3911:ASOCRH>2.0.CO;2.
- , and —, 1988b: A study of cloud-generated radiative heating and its generation of available potential energy. Part II: Results for a climatological zonal mean January. *J. Atmos. Sci.*, **45**, 3928–3943, doi:10.1175/1520-0469(1988)045<3928:ASOGRH>2.0.CO;2.
- Tian, B., and V. Ramanathan, 2002: Role of tropical clouds in surface and atmospheric energy budget. *J. Climate*, **15**, 296–305, doi:10.1175/1520-0442(2002)015<0296:ROTCIS>2.0.CO;2.
- , and —, 2003: A simple moist tropical atmosphere model: The role of cloud radiative forcing. *J. Climate*, **16**, 2086–2092, doi:10.1175/1520-0442(2003)016<2086:ASMTAM>2.0.CO;2.
- , G. J. Zhang, and V. Ramanathan, 2001: Heat balance in the Pacific warm pool atmosphere during TOGA COARE and CEPEX. *J. Climate*, **14**, 1881–1893, doi:10.1175/1520-0442(2001)014<1881:HBITPW>2.0.CO;2.
- Trenberth, K. E., and A. Solomon, 1994: The global heat balance: Heat transports in the atmosphere and ocean. *Climate Dyn.*, **10**, 107–134, doi:10.1007/BF00210625.
- Voigt, A., S. Bony, J.-L. Dufresne, and B. Stevens, 2014: The radiative impact of clouds on the shift of the intertropical convergence zone. *Geophys. Res. Lett.*, **41**, 4308–4315, doi:10.1002/2014GL060354.
- Wielicki, B. A., B. R. Barkstrom, E. F. Harrison, R. B. Lee, G. Louis Smith, and J. E. Cooper, 1996: Clouds and the Earth's

- Radiant Energy System (CERES): An Earth observing system experiment. *Bull. Amer. Meteor. Soc.*, **77**, 853–868, doi:[10.1175/1520-0477\(1996\)077<0853:CATERE>2.0.CO;2](https://doi.org/10.1175/1520-0477(1996)077<0853:CATERE>2.0.CO;2).
- , and Coauthors, 1998: Clouds and the Earth's Radiant Energy System (CERES): Algorithm overview. *IEEE Trans. Geosci. Remote Sens.*, **36**, 1127–1141, doi:[10.1109/36.701020](https://doi.org/10.1109/36.701020).
- Wu, Y., M. Ting, R. Seager, H.-P. Huang, and M. A. Cane, 2011: Changes in storm tracks and energy transports in a warmer climate simulated by the GFDL CM2.1 model. *Climate Dyn.*, **37**, 53–72, doi:[10.1007/s00382-010-0776-4](https://doi.org/10.1007/s00382-010-0776-4).
- Yuan, J., and D. L. Hartmann, 2008: Spatial and temporal dependence of clouds and their radiative impacts on the large-scale vertical velocity profile. *J. Geophys. Res.*, **113**, D19201, doi:[10.1029/2007JD009722](https://doi.org/10.1029/2007JD009722).
- , —, and R. Wood, 2008: Dynamic effects on the tropical cloud radiative forcing and radiation budget. *J. Climate*, **21**, 2337–2351, doi:[10.1175/2007JCLI1857.1](https://doi.org/10.1175/2007JCLI1857.1).
- Zelinka, M. D., and D. L. Hartmann, 2012: Climate feedbacks and their implications for poleward energy flux changes in a warming climate. *J. Climate*, **25**, 608–624, doi:[10.1175/JCLI-D-11-00096.1](https://doi.org/10.1175/JCLI-D-11-00096.1).
- Zhang, Y.-C., and W. B. Rossow, 1997: Estimating meridional energy transports by the atmospheric and oceanic general circulations using boundary fluxes. *J. Climate*, **10**, 2358–2373, doi:[10.1175/1520-0442\(1997\)010<2358:EMETBT>2.0.CO;2](https://doi.org/10.1175/1520-0442(1997)010<2358:EMETBT>2.0.CO;2).